



# Evaluation of micro rain radar-based precipitation classification algorithms to discriminate between stratiform and convective precipitation

Andreas Foth<sup>1</sup>, Janek Zimmer<sup>2</sup>, Felix Lauermann<sup>1,3</sup>, and Heike Kalesse<sup>1</sup>

<sup>1</sup>Leipzig Institute for Meteorology, University of Leipzig, Leipzig, Germany

<sup>2</sup>Meteologix AG, Sattel, Switzerland

<sup>3</sup>now at: Deutscher Wetterdienst, Meteorologisches Observatorium Lindenberg/Richard–Aßmann–Observatorium, Tauche, Germany

**Correspondence:** Andreas Foth (andreas.foth@uni-leipzig.de)

**Abstract.** In this paper, we present two micro rain radar-based approaches to discriminate between stratiform and convective precipitation. One is based on probability density functions (PDFs) in combination with a confidence function and the other one is an artificial neural network (ANN) classification. Both methods use the maximum radar reflectivity per profile, the maximum of the observed mean Doppler velocity per profile and the maximum of the temporal standard deviation ( $\pm 15$  min) of the observed mean Doppler velocity per profile from a micro rain radar (MRR). Training and testing of the algorithms were performed using a two year data set from the Jülich Observatory for Cloud Evolution (JOYCE). Both methods agree well giving similar results. However, the results of the artificial neural network are more reasonable since it is also able to distinguish into an inconclusive class, in turn making the stratiform and convective classes more reliable.

## 10 1 Introduction

Evaporation of precipitation below cloud base is a crucial process in the water- and energy cycle. The parameterization of this process is highly empirical in current general circulation models (Rotstayn, 1997). Evaporation of precipitation generates cold pools that lead to convective organisation (Schlemmer and Hohenegger, 2014) and Tropical storms (Pattnaik and Krishnamurti, 2007); it is highly relevant for boundary-layer humidity (Worden et al., 2007) and subsequently for the Tropical general circulation (Bacmeister et al., 2006). However, also in the midlatitudes, precipitation evaporation is an important factor in the water cycle (Morrison et al., 2012) and the simulated water cycle processes are highly sensitive to the empirical parameters and assumptions.

In order to improve the parameterization of evaporation from convective rain a big data set of convective rain cases is needed to generate robust statistics. Since it is a large effort to manually discriminate between stratiform and convective cases, automated



algorithms were developed.

In previous approaches Caracciolo et al. (2006) separated stratiform and convective rain based on the rain drop size distribution measured by a disdrometer. Precipitation was also classified using radar images and radar wind profiler data (Rosenfeld et al., 1995; Williams et al., 1995; Tokay and Short, 1996; Tokay et al., 1999; Yang et al., 2013). Deng et al. (2014) classified convective precipitation based on thresholds of the radar reflectivity and the gradient of accumulative radar reflectivity retrieved from a vertically pointing cloud radar. Geerts and Dawei (2004) used a decision tree to separate different precipitation types by means of cloud radar variables. Yang et al. (2019) developed a discrimination algorithm using an ANN. Lazri and Ameur (2018) combined a support vector machine, ANN and random forest to improve the stratiform convective classification using spectral features of SEVIRI data.

In summary, several approaches such as ANN, fuzzy logics, or decision trees based on different instruments such as disdrometer, cloud radar, precipitation radar, or radar wind profiler were developed in the past. In this paper, two methods are developed which classify rain as stratiform or convective event based only on MRR observations to enable a wide spread and straightforward usage for ground-based remote-sensing sites.

## 2 Instrumentation

### 2.1 Supersite JOYCE

In recent years, the Jülich Observatory for Cloud Evolution (JOYCE<sup>1</sup>) was equipped with a combination of synergistic ground-based instruments (Löhnert et al., 2015). JOYCE is situated at 50°54'31"N and 6°24'49"E with an altitude of 111 m MSL. In 2017 JOYCE was transformed into a Core Facility (JOYCE – CF) funded by the DFG (Deutsche Forschungsgemeinschaft) with the aim of high quality radar and passive microwave observations of the atmosphere. The supersite operates a variety of ground-based active and passive remote sensing instruments for cloud and precipitation observations, for example: X, Ka, and W-Band radars, ceilometers, a Doppler wind lidar, an atmospheric emitted radiance interferometer (AERI), a Sun photometer, disdrometers, several radiation measurement systems, as well as an MRR. The latter is the main instrument in this study and is explained in detail in the following section. The data used in this study was gathered in 2013 and 2014. The data from 2013 covers the entire year and was used to train the algorithms (training data set). The data from 2014 covers almost the entire year apart from February. It is completely independent and is used as test data set for the algorithms. In 2013 and 2014, 471 and 683 hours of rain were observed, respectively.

<sup>1</sup>JOYCE webpage: [http://cpex-lab.de/cpex-lab/EN/Home/JOYCE-CF/JOYCE-CF\\_node.html](http://cpex-lab.de/cpex-lab/EN/Home/JOYCE-CF/JOYCE-CF_node.html), last accessed: 2020-07-16



## 2.2 Micro rain radar

The micro rain radar (MRR) which is built by the Metek (Meteorologische Messtechnik GmbH) company, is a compact FM-CW (frequency modulated-continuous wave) Doppler radar operating at 24 GHz (Peters et al., 2002). The MRR at JOYCE (in 2013 and 2014) was operated with 31 range gates from 100 to 3100 m resulting in a vertical resolution of 100 m. The temporal resolution amounted to 1 min. The MRR data was processed according to Peters et al. (2005). The instrument was zenith pointing and measured the radar Doppler spectrum from which the attenuated equivalent reflectivity  $Z$  and the mean Doppler velocity were derived.

## 3 Stratiform convective discrimination

### 3.1 Convection indices

Several weather indices can be used to describe the stability of the atmosphere (Kunz, 2007). Three indices are described in the following. All give a hint on the probability of convection based on COSMO (Consortium for Small-scale Modeling) model data. The total totals is a combination of the vertical totals ( $VT$ ) and cross totals ( $CT$ ). The  $VT$  is the temperature ( $\vartheta$  in ° Celsius) difference between 850 hPa and 500 hPa while the  $CT$  is 850 hPa dewpoint ( $\tau$ ) minus the 500 hPa temperature:

$$\begin{aligned} TT &= VT + CT \\ &= (\vartheta_{850} - \vartheta_{500}) + (\tau_{850} - \vartheta_{500}). \end{aligned} \quad (1)$$

The higher the  $TT$ , the more probable is convection.

The second index, named KO index (Andersson et al., 1989), describes the potential instability between lower and higher levels of the atmosphere (at 1000 hPa, 850 hPa, 700 hPa, and 500 hPa). It is thus based on the pseudo-potential temperatures  $\theta_e$

$$KO = 0.5(\theta_{e,700} + \theta_{e,500} - \theta_{e,1000} - \theta_{e,850}). \quad (2)$$

The lower the  $KO$  index the higher the probability of convection.

The soaring index<sup>2</sup> ( $S$ ) is intended to be a tool in soaring and sporting aviation because it gives a hint on thermal lift and hence on instability. It is defined as:

$$S = \vartheta_{850} - \vartheta_{500} + \tau_{500} - (\vartheta_{700} + \tau_{700}). \quad (3)$$

The higher the  $S$  index the higher the probability of convection.

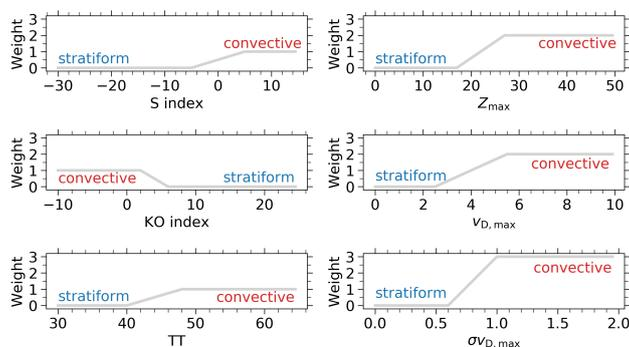


**Figure 1.** Weight of the meteorological and radar-based convection criteria: soaring index ( $S$ ), convection index ( $Ko$ ), total totals ( $TT$ ), maximum of the reflectivity ( $Z_{\max}$ ) per profile, maximum of the Doppler velocity ( $v_{D,\max}$ ) per profile and the maximum (per profile) of the temporal standard deviation of the Doppler velocity ( $\sigma v_{D,\max}$ ) within a  $\pm 15$  min interval.

### 3.2 Convection score

First, a convection score to classify three types of precipitation, stratiform, convective and inconclusive, is defined by applying a threshold range to six different variables. Three variables are based on thermodynamic profiles ( $S$ ,  $KO$ ,  $TT$ ) and three are based on the MRR observations. Specifically, the used MRR variables are: the maximum of reflectivity ( $Z_{\max}$ ) per profile, maximum of the mean Doppler velocity ( $v_{D,\max}$ ) per profile and the maximum (per profile) of the temporal standard deviation ( $\pm 15$  min) of the mean Doppler velocity ( $\sigma v_{D,\max}$ ). It is expected that convective precipitation contains larger rain drops resulting in higher  $Z$  and  $v_D$  values, respectively. Furthermore, stratiform precipitation is expected to be less variable over time whereas convective precipitation results in a larger standard deviation of  $v_D$  over time. It was shown that  $\pm 15$  min is a reasonable time span for classification of rain events. The maxima of the height dependent  $Z$ ,  $v_D$  and  $\sigma v_D$  are used to assign the vertical properties to profile properties.

The variables have different weightings visualized in Fig. 1. Whenever a variable exceeds a convection threshold range (or falls below in case of  $KO$  index), the weight to be convective increases. The weightings of all variables are summed up resulting in the convection score. The application of a smooth linear threshold range of weights between stratiform and convective is more realistic than using strict binary thresholds which finally leads to a more homogeneous distribution of the convection score. By using six variables the classification is more robust against false classifications than those based on one single variable. The MRR-based variables have a stronger weighting than the model-based variables due to their smaller uncertainties. The weight of  $\sigma v_{D,\max}$  has the highest weight because the variability of the rain intensity is assumed to be the best criterion for the stratiform-convective discrimination.

Figure 2 illustrates the distribution of the convection score. Whenever a convection score is less than 3 the profile is assigned

<sup>2</sup>[http://www2.wetter3.de/soaring\\_index.html](http://www2.wetter3.de/soaring_index.html), last accessed: 2020-07-16

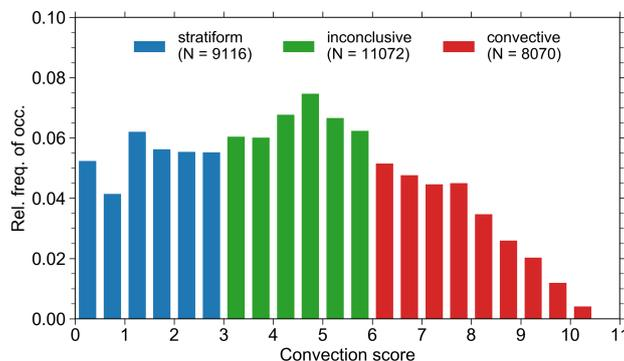


**Figure 2.** Relative frequency of occurrence of the convective score.

to be stratiform. Values between 3 and 6 are stated as inconclusive. Values larger than or equal to 6 are assigned as convective. These strict thresholds enable a very certain classification with a low amount of false classifications. This approach replaces a manual classification by visual classification of each single profile. However, several rain events were reviewed by eye to verify a correct classification.

5

At this step, each profile is either classified as stratiform, inconclusive, or convective using the convection score and this assignment is stated as true state to train the algorithms explained below. Since the motivation of this work is to classify the precipitation type and its confidence only based on the MRR observations the following methods based on PDFs or ANN are deployed. Since the PDF and ANN method are based on training, the data has to be free of extreme or unphysical values.

10 Therefore the data is filtered. Only measurements with  $Z_{\max}$  between -10 and 50 dBZ,  $v_{D,\max}$  between 0 and  $10 \text{ m s}^{-1}$  and  $\sigma v_{D,\max}$  between 0 and  $2.5 \text{ m s}^{-1}$  are taken into account.

Here, the question might arise why inconclusive profiles should be learned by algorithms. In fact, rain events can be ambiguous and cannot be classified into stratiform or convective, especially stratiform rain moving towards mountainous area which causes convection. On the other hand, vertical air motion and turbulence influence  $v_{D,\max}$  and might shift stratiform profiles towards higher convection scores and convective profiles to lower scores. A class with inconclusive profiles accounts for the mentioned features and avoids misclassifications into the stratiform and convective classes, respectively.

15

### 3.3 Rain classification method based on PDF

20 This algorithm was developed based on the classification algorithms by Liu et al. (2004) and Liu et al. (2009) which were originally developed for the Cloud-Aerosol Lidar and Infrared Pathfinder Satellite Observations (CALIPSO) aerosol cloud discrimination (Winker et al., 2009). It shows that the confidence of a discrimination algorithm can be improved by using three measurement variables instead of only one or two. Here, this approach is modified for MRR variables to classify precipitation

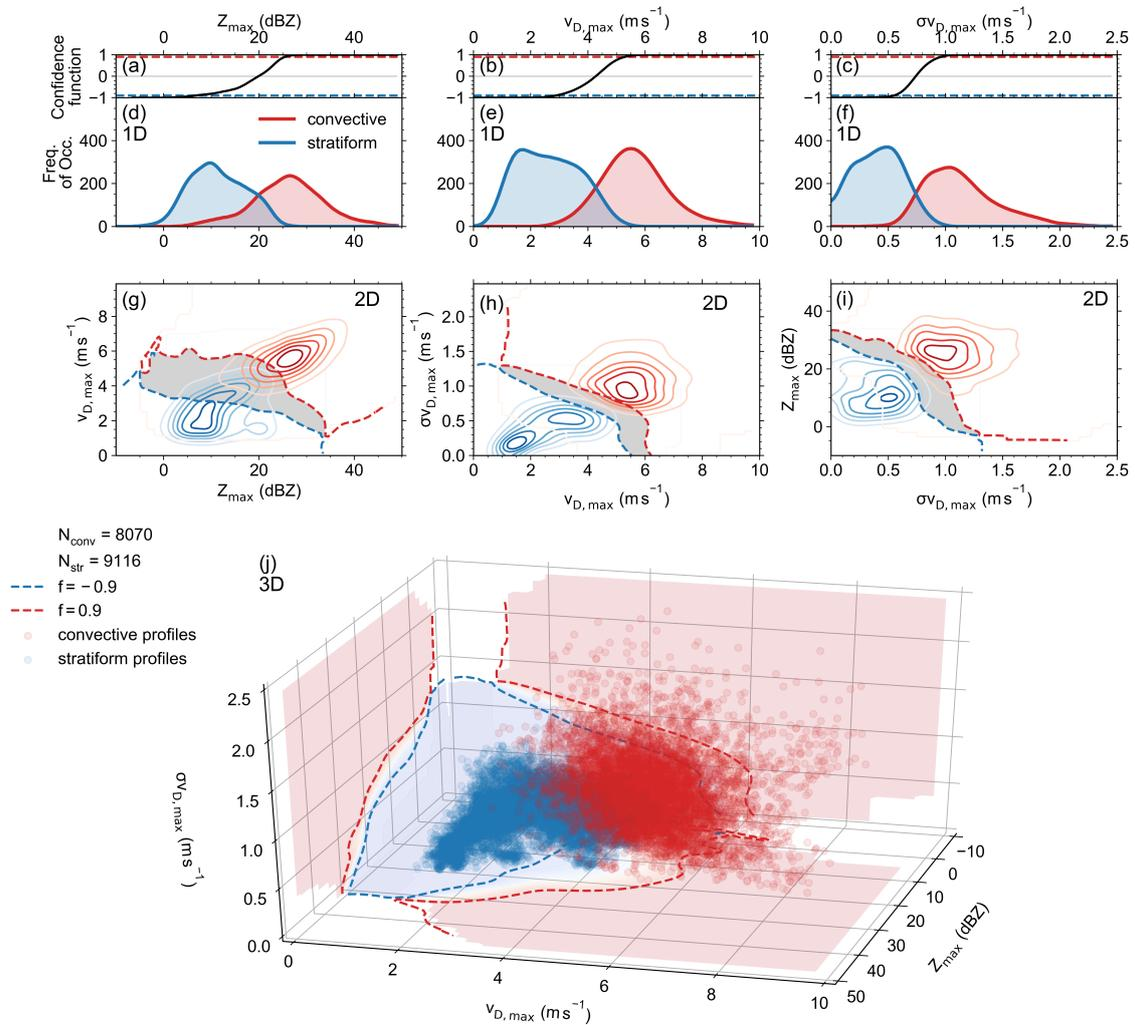


**Figure 3.** Overview about the one-dimensional (1D,d,e,f), two-dimensional (2D,g,h,i), and three-dimensional (3D,j) probability density functions for the maximum radar reflectivity  $Z_{\max}$  per profile (d), the of the observed Doppler velocity  $v_{D,\max}$  per profile (e), the maximum of the temporal standard deviation of the observed Doppler velocity  $\sigma_{v_{D,\max}}$  per profile (f), and each 2D combination of these three variables (g-i). (j) shows the 3D scatterplot of the three variables with the contour of the corresponding confidence values in each plane. (a-c) show the the confidence function of the corresponding 1D distributions. The dashed lines represent the thresholds of a confident classification with values beyond -0.9 and 0.9, whereas values in between are indicated by a grey area (g-i). Stratiform or convective profiles are indicated by blue or red colours and by low or high values of the confidence functions, respectively.

into stratiform or convective.



The confidence function is defined as:

$$f(\mathbf{X}) = \frac{n_c(\mathbf{X}) - n_s(\mathbf{X})}{n_c(\mathbf{X}) + n_s(\mathbf{X})} \quad (4)$$

$$= \frac{P_c(\mathbf{X}) - P_s(\mathbf{X})/N_s/N_c}{P_c(\mathbf{X}) + P_s(\mathbf{X})/N_s/N_c} \quad (5)$$

with  $n_i$  being the number of occurrences of class  $i$  (stratiform  $s$  or convective  $c$ ) having attribute  $X$  and  $N_i$  the total number of events for the  $i$ th class.  $P$  is the PDF of  $\mathbf{X}$  which can be multidimensional  $\mathbf{X} = [X_1, \dots, X_m]$ . The value of  $f$  is bounded on  $[-1, 1]$ . The lower the value, the more probable the MRR-observed rain profile is to be stratiform. Values of exactly  $-1$  are treated as certainly stratiform and values of  $+1$  correspond to certainly convective profiles. Values around 0 indicate uncertain classifications. On the basis of the return value of  $f$  a classification and a measure of the confidence of this classification can be derived. The sign of  $f$  determines the class assignment and the absolute magnitude of  $f$  assigns the confidence to the classification. In the following the PDFs are smoothed using a Gaussian filter with a standard deviation of 3 bins in each dimension to account for gaps in the PDF due to missing variable combination in the training data. Applying such a filter makes the PDF method more robust.

Figure 3 (d), (e) and (f) shows the one-dimensional distribution of the three MRR variables ( $Z_{\max}$ ,  $v_{D,\max}$  and  $\sigma v_{D,\max}$ ) and their corresponding confidence functions  $f$  (a,b,c). Here, the stratiform and convective precipitation profiles are distinguished by the convection score explained above. However,  $Z_{\max}$  at values between 5 and 25 dB shows a region of overlap between both classes resulting in low magnitude of  $f$  with values between  $-0.8$  and  $0.8$ .  $Z_{\max}$  below 5 dB or above 25 dB can be reliably classified as stratiform or convective, respectively (Fig. 3 d). The distribution of  $v_{D,\max}$  (Fig. 3 e) as well as  $\sigma v_{D,\max}$  (Fig. 3 f) shows a significant overlap region between 2.5 and 5.5  $\text{m s}^{-1}$  and between 0.2 and 0.8  $\text{m s}^{-1}$ , respectively. This results in absolute magnitudes of  $f$  below 0.8. Since vertical air motion and turbulence influence  $v_{D,\max}$ , it thus can not serve as stand-alone value. In conclusion, a classification algorithm based on only one of the mentioned MRR variables is not able to unambiguously distinguish between stratiform and convective precipitation indicated by the overlap regions.

The ambiguity can be reduced by adding a second dimension to the PDF. Figure 3 (g), (h) and (i) illustrate the distribution of each two-dimensional (2D) combination of the three MRR-based variables. The dashed lines indicate the  $f$  values of  $-0.9$  and  $0.9$ . The values in between represent the overlap where no unambiguous assignment can be made (grey area). The peaks of the two classes are clearly separated for all three variable combinations (g,h,i). Nevertheless, there are still observations leading to an ambiguous assignment. In principle, these ambiguous assigned profiles with  $f$  values between  $-0.9$  and  $0.9$  could be stated as inconclusive. However, the PDF algorithm is not trained to classify inconclusive cases. A quantitative estimation of how well the discrimination works is given at the end of this section.

By using all three mentioned MRR-based variables a three-dimensional (3D) PDF can be created which is visualized in Fig. 3 (j). It is indicated that both stratiform and convective profiles are clearly separated with a very small region of overlap. The quality of the 3D PDF-based classification in contrast to 2D and 1D can be explained in terms of failure rates  $R_f$  (Liu

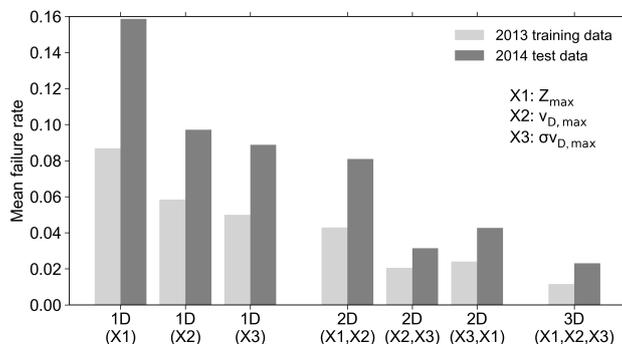


**Figure 4.** The mean stratiform convective discrimination failure rates contrasted between two data sets, training data 2013 (light grey) and test data 2014 (dark grey). The shown failure rate is separated for PDFs with increasing dimension: 1D is based on only one MRR variable, 2D is a two dimensional PDF based on two MRR variables and, 3D is a three dimensional PDF based on three MRR variables, as mentioned in the legend.

et al., 2009):

$$R_f(\mathbf{X}) = \frac{|f(\mathbf{X}) - 1|}{-2}. \quad (6)$$

As explained above the performance of the classification is limited by the amount of overlap in the PDFs. The smaller the overlap, the more clear is the separation between stratiform and convective profiles. Figure 4 presents the mean failure rate for the 1D-, 2D-, and 3D PDFs of training data set 2013 and the independent test data set 2014. The training data was used to build the PDF for the calculation of  $f$ . For each profile from the test data, the according  $f$  value can be read out from the trained confidence function. To account for measurement uncertainties and turbulence influencing all radar variables, the  $f$  underlying PDFs are smoothed using a Gaussian filter with a standard deviation of 3 bins in each dimension corresponding to a  $Z_{\max}$  of 1.5 dB,  $v_{D,\max}$  of  $0.38 \text{ ms}^{-1}$ , and  $\sigma v_{D,\max}$  of  $0.08 \text{ ms}^{-1}$ . It can be seen that a reduction of the overlap by adding another attribute (MRR-based variable) results in smaller failure rates. The mean failure rate for the 3D-PDF based rain classification discrimination for training and test data is less than 1 % and 3 %, respectively. This is much lower than the failure rates of 1D and 2D PDFs for stratiform-convective discrimination, which range between 2 to 9 % for the training data set and 3 to 16 % for the test data set.

### 15 3.4 Method based on an artificial neural network (ANN)

A classification of rain as stratiform, convective or inconclusive can also be based on an ANN. The ANN model is a multi-layer perceptron approach implemented using the open source machine learning library for research and production *TensorFlow*<sup>3</sup>. It is trained with  $Z_{\max}$ ,  $v_{D,\max}$  and  $\sigma v_{D,\max}$  from the training data set (2013). The ANN model (Fig. 5) consists of 3 input nodes ( $Z_{\max}$ ,  $v_{D,\max}$  and  $\sigma v_{D,\max}$ ) and is further composed of two hidden layers with 6 nodes each, and one output node to learn how

<sup>3</sup>TensorFlow: An end-to-end open source machine learning platform, <https://www.tensorflow.org/>, last accessed: 2020-07-16

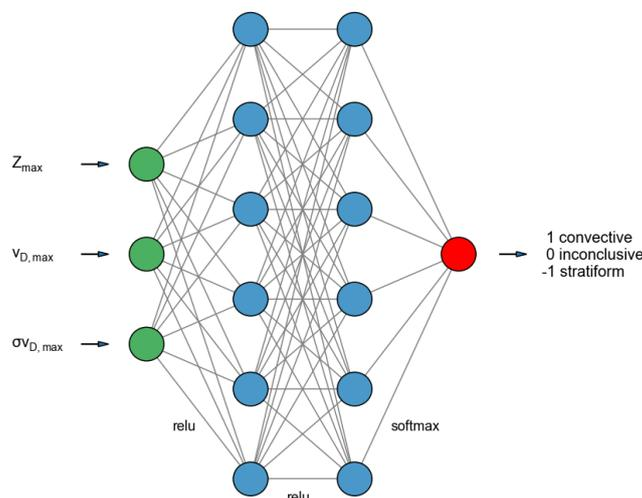


**Figure 5.** Diagram of the neural network with an input layer consisting of three nodes (green) according to the three MRR-based variables, two hidden layers with six nodes each (blue) and the output layer with one node (red).

to classify rain events according to the true classification made by the convection score. The model is trained for 300 epochs (iteration steps) and the training data is shuffled before each epoch. The algorithm *Adam*<sup>4</sup> is used to optimize the model. As activation functions *relu* (rectified linear unit) and *softmax* are used for the two hidden layers and the output layer, respectively. *Relu* avoids negative output whereas *softmax* produces an output which is a range of values between 0 and 1, with the sum of the probabilities been equal to 1. As loss function the categorical cross-entropy is used to compute the cross-entropy loss between the truth and the predictions. The cross-entropy is a measure of the difference between two probability distributions. The accuracy of the neural network can be described in terms of how often the predictions equals the truth. The ANN accuracy referred to a validation data set, which is a subset of a tenth of randomly chosen 2013 data, exceeds 92%. Giving  $Z_{\max}$ ,  $v_{D,\max}$  and  $\sigma_{v_{D,\max}}$  as input to the ANN it will classify the rain event with a probability to be stratiform (labeled as  $-1$ ), inconclusive (0) or convective (1).

## 4 Results

After the successful development and evaluation of the classification algorithms, both 3D-PDF-based and ANN were applied to two case studies. The first one was a rainy day on 11 Feb 2013 (Fig. 6 a-g). Figure 6 (e) shows the time–height display of the attenuated equivalent reflectivity. During the day there were four rain events at around 6:00, 10:00, 11:00 and 15:00 UTC. The rain fell homogeneously with quite constant  $Z_{\max}$  (a),  $v_{D,\max}$  (b) and  $\sigma_{v_{D,\max}}$  (c). The calculated convection score (d) was very low which means that these rain events were stated to be stratiform. The PDF-based algorithm classifies each single profile as stratiform apart from two outliers at 12:30 UTC (Fig. 6 f). The ANN classifies all profiles as stratiform except for the outliers

<sup>4</sup>Kingma, D.P. and Ba, J.: Adam: A Method for Stochastic Optimization, 2014. web: <https://arxiv.org/abs/1412.6980>

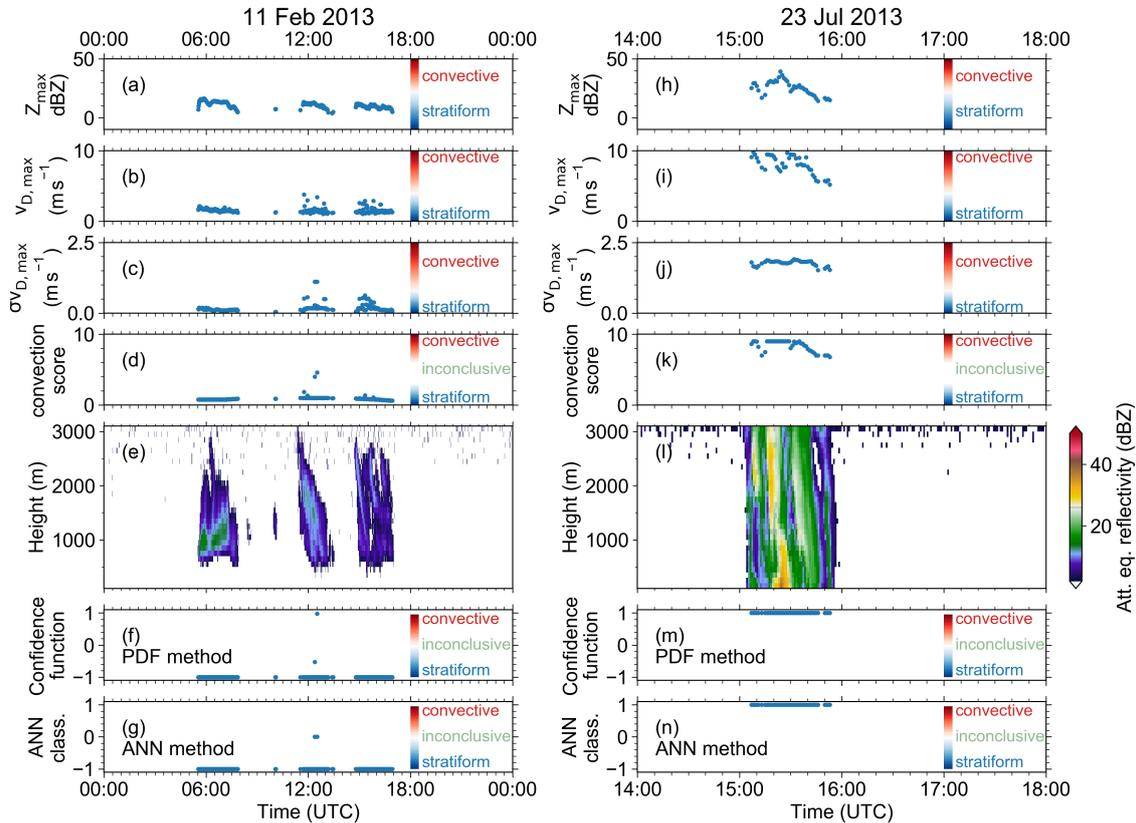


**Figure 6.** Discrimination indices:  $Z_{\max}$  (a,h),  $v_{D,\max}$  (b,i),  $\sigma v_{D,\max}$  (c,j) and the convection score indicating the true rain type (d,k). MRR reflectivity (e,l) and the rain classification based on the PDF method given by the confidence function (f,m) and based on the ANN (g,n). The color bars within the time series illustrate whether the values indicate stratiform or convective rain. Left panels are from 11 February 2013 and the right panels are from 23 July 2013.

from the PDF method. Those are classified as inconclusive which is more reasonable in this context. For these wintertime rain events, the ANN and PDF method produce very similar results and both agree with the true class given by the convection score.

The right panel of Fig. 6 shows the same quantities as on the left panel but for 23 July 2013. In contrast to the presented winter case, this case indicates convective rain represented at 15:00 UTC.  $Z_{\max}$  (h),  $v_{D,\max}$  (i) and  $\sigma v_{D,\max}$  (j) and the calculated convection score are characterized by high values representing convective rain. (l) gives an impression on the attenuated equivalent reflectivity of the shower and its short intense time span. Both methods are in a very good agreement and classify each profile as convective in conformity with the convection score (truth).

The performance of both algorithms over a whole year (test data year 2014) is illustrated in Fig. 7. The relative frequency of occurrence of the stratiform cases from PDF and ANN values agrees well within a few percent. 23 % of inconclusive cases

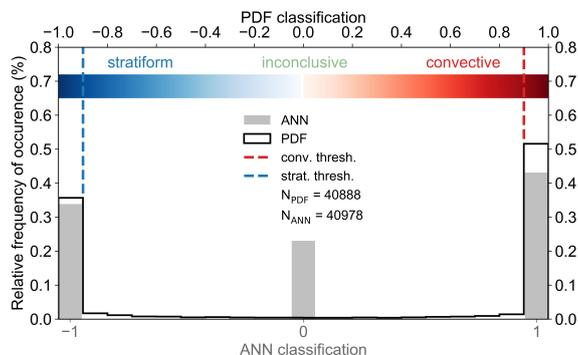


**Figure 7.** Relative Frequency of occurrences of stratiform, inconclusive and convective rain classification for both PDF (black) and ANN (grey) method based on the test data 2014. The color bar on the top indicates the confidence of the classification. The more blue or red the color is the more confident the rain profile is classified as stratiform or convective. The dashed lines indicate the thresholds for stratiform and convective classifications. The numbers denote the sample size.

classified by the ANN are contrasted by 13 % from PDF method. The lower amount of inconclusive cases at the PDF method is caused by the fact, that this class is actually not distinguished, since it is classified as uncertain stratiform convective discrimination ( $f$  value between  $-0.9$  and  $0.9$ ). The difference between both methods for convective cases amounts to 8 %. One has to consider that the total amount of data is different for both methods. This is due to the fact that some combinations of the three input variables do not appear within the training data causing gaps in the 3D PDF. Those combinations cannot be classified.

## 5 Conclusions and outlook

In order to improve microphysical parametrizations within small-scale models one has to deal with large data sets. The presented rain type classification methods based on PDF and ANN algorithms are suited to process micro rain radar data from long time series and outperform traditional convective score methods. The effort of creating a robust training data set without unphysical data between both methods is similar and the application of both methods is straightforward. The main advantage of the ANN in contrast to the PDF method is that inconclusive profiles can be classified which leads to a lower amount of false classified profiles. In a next step, evaporative cooling rates will be estimated for convective rain events to parametrize the cooling by means of temperature, relative humidity and rain droplet number concentration. It is also planned to apply the algorithms to different ground-based remote-sensing sites that have long-term MRR observations to create stratiform-vs-convective rain event climatologies.

*Code availability.* The open source machine learning library for research and production TensorFlow (Abadi et al., 2015) used for this publication is available under <https://www.tensorflow.org/>, last accessed: 2020-07-16.



*Author contributions.* AF prepared the manuscript in close collaboration with HK. AF performed the investigations and data analyses. JZ and FL contributed with their knowledge about basic meteorology and convective indices. JZ also contributed with his experience in radar data analysis. The conceptualization was initialized by AF. All authors have contributed to the scientific discussions.

*Competing interests.* The authors declare that they have no conflict of interest.

- 5 *Acknowledgements.* This research has been supported by German Science Foundation (DFG) through funding the grants FO 1285/2-1, KA 4162/2-1 (PICNICC within the priority programme PROM) and WE 1900/33-1 and the Federal Ministry of Education and Research in Germany (BMBF) through High-Definition Clouds and Precipitation for advancing Climate Prediction research programme (HD(CP)2; FKZ: 01LK1504C and 01LK1502N). Data from JOYCE were provided by DFG-funded Core Facility (JOYCE-CF) under DFG research grant LO 901/7-1.



## References

- Abadi, M., Agarwal, A., Barham, P., Brevdo, E., Chen, Z., Citro, C., Corrado, G. S., Davis, A., Dean, J., Devin, M., Ghemawat, S., Goodfellow, I., Harp, A., Irving, G., Isard, M., Jia, Y., Jozefowicz, R., Kaiser, L., Kudlur, M., Levenberg, J., Mané, D., Monga, R., Moore, S., Murray, D., Olah, C., Schuster, M., Shlens, J., Steiner, B., Sutskever, I., Talwar, K., Tucker, P., Vanhoucke, V., Vasudevan, V., Viégas, F., Vinyals, O., Warden, P., Wattenberg, M., Wicke, M., Yu, Y., and Zheng, X.: TensorFlow: Large-Scale Machine Learning on Heterogeneous Systems, <https://www.tensorflow.org/>, software available from tensorflow.org, 2015.
- Andersson, T., Andersson, M., Jacobsson, C., and Nilsson, S.: Thermodynamic indexes for forecasting thunderstorms in southern sweden, *Meteorol. Mag.*, 118, 141–146, 1989.
- Bacmeister, J. T., Suarez, M. J., and Robertson, F. R.: Rain Reevaporation, Boundary Layer–Convection Interactions, and Pacific Rainfall Patterns in an AGCM, *Journal of the Atmospheric Sciences*, 63, 3383–3403, <https://doi.org/10.1175/JAS3791.1>, <https://doi.org/10.1175/JAS3791.1>, 2006.
- Caracciolo, C., Prodi, F., Battaglia, A., and Porcu, F.: Analysis of the moments and parameters of a gamma DSD to infer precipitation properties: A convective stratiform discrimination algorithm, *Atmos. Res.*, 80, 165 – 186, <https://doi.org/https://doi.org/10.1016/j.atmosres.2005.07.003>, <http://www.sciencedirect.com/science/article/pii/S0169809505002097>, 2006.
- Deng, M., Kollias, P., Feng, Z., Zhang, C., Long, C. N., Kalesse, H., Chandra, A., Kumar, V. V., and Protat, A.: Stratiform and Convective Precipitation Observed by Multiple Radars during the DYNAMO/AMIE Experiment, *J. Appl. Meteorol. Clim.*, 53, 2503–2523, <https://doi.org/10.1175/JAMC-D-13-0311.1>, <https://doi.org/10.1175/JAMC-D-13-0311.1>, 2014.
- Geerts, B. and Dawei, Y.: Classification and Characterization of Tropical Precipitation Based on High-Resolution Airborne Vertical Incidence Radar. Part I: Classification, *J. Appl. Meteorol.*, 43, 1554–1566, <https://doi.org/10.1175/JAM2158.1>, <https://doi.org/10.1175/JAM2158.1>, 2004.
- Kunz, M.: The skill of convective parameters and indices to predict isolated and severe thunderstorms, *Nat. Hazard Earth Sys.*, 7, 327–342, <https://doi.org/10.5194/nhess-7-327-2007>, 2007.
- Lazri, M. and Ameer, S.: Combination of support vector machine, artificial neural network and random forest for improving the classification of convective and stratiform rain using spectral features of SEVIRI data, *Atmos. Res.*, 203, 118 – 129, <https://doi.org/https://doi.org/10.1016/j.atmosres.2017.12.006>, <http://www.sciencedirect.com/science/article/pii/S0169809517309572>, 2018.
- Liu, Z., Vaughan, M. A., Winker, D. M., Hostetler, C. A., Poole, L. R., Hlavka, D., Hart, W., and McGill, M.: Use of probability distribution functions for discriminating between cloud and aerosol in lidar backscatter data, *J. Geophys. Res. Atmos.*, 109, D15202, <https://doi.org/10.1029/2004JD004732>, 2004.
- Liu, Z., Vaughan, M., Winker, D., Kittaka, C., Getzewich, B., Kuehn, R., Omar, A., Powell, K., Trepte, C., and Hostetler, C.: The CALIPSO Lidar Cloud and Aerosol Discrimination: Version 2 Algorithm and Initial Assessment of Performance, *J. Atmos. Oceanic Technol.*, 26, 1198–1213, <https://doi.org/10.1175/2009JTECHA1229.1>, 2009.
- Löhnert, U., Schween, J. H., Acquistapace, C., Ebell, K., Maahn, M., Barrera-Verdejo, M., Hirsikko, A., Bohn, B., Knaps, A., O’Connor, E., Simmer, C., Wahner, A., and Crewell, S.: JOYCE: Jülich Observatory for Cloud Evolution, *Bulletin of the American Meteorological Society*, 96, 1157–1174, <https://doi.org/10.1175/BAMS-D-14-00105.1>, 2015.



- Morrison, H., Tessendorf, S. A., Ikeda, K., and Thompson, G.: Sensitivity of a Simulated Midlatitude Squall Line to Parameterization of Raindrop Breakup, *Monthly Weather Review*, 140, 2437–2460, <https://doi.org/10.1175/MWR-D-11-00283.1>, <https://doi.org/10.1175/MWR-D-11-00283.1>, 2012.
- Pattnaik, S. and Krishnamurti, T. N.: Impact of cloud microphysical processes on hurricane intensity, part 2: Sensitivity experiments, *Meteorology and Atmospheric Physics*, 97, 127–147, <https://doi.org/10.1007/s00703-006-0248-x>, <https://doi.org/10.1007/s00703-006-0248-x>, 2007.
- Peters, G., Fischer, B., and Anderson, T.: Rain observations with a vertically looking Micro Rain Radar (MRR), *Boreal Environ. Res.*, 7, 353–362, 2002.
- Peters, G., Fischer, B., Münster, H., Clemens, M., and Wagner, A.: Profiles of Raindrop Size Distributions as Retrieved by Microrain Radars, 44, 1930–1949, <https://doi.org/10.1175/JAM2316.1>, 2005.
- Rosenfeld, D., Amitai, E., and Wolff, D. B.: Improved Accuracy of Radar WPMM Estimated Rainfall upon Application of Objective Classification Criteria, *J. Appl. Meteorol.*, 34, 212–223, <https://doi.org/10.1175/1520-0450-34.1.212>, <https://doi.org/10.1175/1520-0450-34.1.212>, 1995.
- Rotstain, L. D.: A physically based scheme for the treatment of stratiform clouds and precipitation in large-scale models. I: Description and evaluation of the microphysical processes, *Quarterly Journal of the Royal Meteorological Society*, 123, 1227–1282, <https://doi.org/10.1002/qj.49712354106>, 1997.
- Schlemmer, L. and Hohenegger, C.: The Formation of Wider and Deeper Clouds as a Result of Cold-Pool Dynamics, *Journal of the Atmospheric Sciences*, 71, 2842–2858, <https://doi.org/10.1175/JAS-D-13-0170.1>, 2014.
- Tokay, A. and Short, D. A.: Evidence from Tropical Raindrop Spectra of the Origin of Rain from Stratiform versus Convective Clouds, *J. Appl. Meteorol.*, 35, 355–371, [https://doi.org/10.1175/1520-0450\(1996\)035<0355:EFTRSO>2.0.CO;2](https://doi.org/10.1175/1520-0450(1996)035<0355:EFTRSO>2.0.CO;2), [https://doi.org/10.1175/1520-0450\(1996\)035<0355:EFTRSO>2.0.CO;2](https://doi.org/10.1175/1520-0450(1996)035<0355:EFTRSO>2.0.CO;2), 1996.
- Tokay, A., Short, D. A., Williams, C. R., Ecklund, W. L., and Gage, K. S.: Tropical Rainfall Associated with Convective and Stratiform Clouds: Intercomparison of Disdrometer and Profiler Measurements, *J. Appl. Meteorol.*, 38, 302–320, [https://doi.org/10.1175/1520-0450\(1999\)038<0302:TRAWCA>2.0.CO;2](https://doi.org/10.1175/1520-0450(1999)038<0302:TRAWCA>2.0.CO;2), [https://doi.org/10.1175/1520-0450\(1999\)038<0302:TRAWCA>2.0.CO;2](https://doi.org/10.1175/1520-0450(1999)038<0302:TRAWCA>2.0.CO;2), 1999.
- Williams, C. R., Ecklund, W. L., and Gage, K. S.: Classification of Precipitating Clouds in the Tropics Using 915-MHz Wind Profilers, *J. Atmos. Ocean. Technol.*, 12, 996–1012, [https://doi.org/10.1175/1520-0426\(1995\)012<0996:COPCIT>2.0.CO;2](https://doi.org/10.1175/1520-0426(1995)012<0996:COPCIT>2.0.CO;2), [https://doi.org/10.1175/1520-0426\(1995\)012<0996:COPCIT>2.0.CO;2](https://doi.org/10.1175/1520-0426(1995)012<0996:COPCIT>2.0.CO;2), 1995.
- Winker, D. M., Vaughan, M. A., Omar, A., Hu, Y., Powell, K. A., Liu, Z., Hunt, W. H., and Young, S. A.: Overview of the CALIPSO Mission and CALIOP Data Processing Algorithms, *J. Atmos. Oceanic Technol.*, 26, 2310–2323, <https://doi.org/10.1175/2009JTECHA1281.1>, 2009.
- Worden, J., Noone, D., Bowman, K., Beer, R., Eldering, A., Fisher, B., Gunson, M., Goldman, A., Herman, R., Kulawik, S. S., Lampel, M., Osterman, G., Rinsland, C., Rodgers, C., Sander, S., Shephard, M., Webster, C. R., Worden, H., science team, and data contributors, T. T. E. S.: Importance of rain evaporation and continental convection in the tropical water cycle, *Nature*, 445, 528–532, <https://doi.org/10.1038/nature05508>, 2007.
- Yang, Y., Chen, X., and Qi, Y.: Classification of convective/stratiform echoes in radar reflectivity observations using a fuzzy logic algorithm, *J. Geophys. Res. Atmos.*, 118, 1896–1905, <https://doi.org/10.1002/jgrd.50214>, <https://agupubs.onlinelibrary.wiley.com/doi/abs/10.1002/jgrd.50214>, 2013.

<https://doi.org/10.5194/amt-2020-290>  
Preprint. Discussion started: 18 August 2020  
© Author(s) 2020. CC BY 4.0 License.



Yang, Z., Liu, P., and Yang, Y.: Convective/Stratiform Precipitation Classification Using Ground-Based Doppler Radar Data Based on the K-Nearest Neighbor Algorithm, *Remote Sens.*, 11, 2277, 2019.